Available at
http://pvamu.edu/aam
Appl. Appl. Math.
ISSN: 1932-9466

Vol. 6, Issue 1 (June 2011) pp. 11 – 26
(Previously, Vol. 6, Issue 11, pp. 1751 – 1766)

Applications and Applied Mathematics:
An International Journal
(AAM)

Mathematical Modeling and Computation of Channel Flow over Discrete Structures

Rolando J. Olivares and Daniel N. Riahi

Department of Mathematics
University of Texas-Pan American
1201 W. University Dr.
Edinburg, Texas 78539-2999 USA
driahi@utpa.edu

Received: June 04, 2010; Accepted: January 26, 2011

Abstract

In this paper mathematical modeling and computation of channel flow over small discrete structures are carried out under some reasonable conditions. A mathematical model for such a flow problem, which is based on a relevant system of partial differential equations and Fourier analysis, is studied using perturbation and nonlinear stability methods, and the resulting flow solutions over two types of discrete structures are computed under both stable and unstable conditions. It was found, in particular, that for a subcritical domain with the Reynolds number R slightly less than its critical value R_c, which is defined as the value below which no disturbances are linearly unstable, the structure leads to a stable steady flow whose modal representations have horizontal scale(s) that are due to those of the structure. On the limiting boundary between the stable and unstable flow, the flow is oscillatory with length scales due to the structure and the critical flow. Larger height of the structure affects the flow more significantly by reducing the subcritical domain for the induced steady flow.

Keywords: Air flow, shear flow, flow forces, viscous flow, flow stability, shear forces, flow modeling, flow instability

MSC 2010 No.: 76E05, 76E99

1. Introduction

This paper considers a relatively simple mathematical model of channel flows over two types of small discrete structure, analyzes the problem, provides the method of solution to the associated system of partial differential equations and presents the results.

It was known for over several decades that surface corrugations and roughness elements can affect flow stabilities and transition to turbulence (Schlichting, 1979; Morkovin, 1983). Other experimental studies (Muller and Bippes, 1988; Rodeztsky et al., 1994) indicated that stationary shear flow modes can be caused or manipulated by the roughness and waviness of the surface and that shear flow modes can be enhanced by selected boundary perturbations. There have been a number of experiments and numerical simulation studies in the past three decades or so (Krettenauer and Schumann, 1992; Hudson et al., 1996; Angelis et al., 1997; Tomkin, 2000) that have suggested significant affects of roughness element or surface waviness on the near wall of turbulent shear flow structures. Tomkins (2000) investigated experimentally turbulent flow in the presence of hemispheres on the wall. The increase in wall friction over the rough surface was found to cause a decrease in the turbulence fluctuations. The roughness elements with larger height affected the flow more significantly than those with smaller height. Vortices generated by the roughness elements were found to take on the scale of the roughness elements. Also streamwise length-scales were found to be reduced due to the presence of roughness elements.

Some related research studies, which were carried out by the second author in the past, are briefly described as follows. Riahi (1997) investigated theoretically the stability of rotating disk boundary layer flow over a simple rough surface using weakly nonlinear method (Drazin and Reid, 1981). It was found, in particular, that certain new types of solutions can become preferred only for particular forms of the amplitude and length scale of the surface roughness. Riahi (2001) investigated the qualitative effect of a corrugated boundary on the laminar shear flow. He found, in particular, that a resonance condition can lead to preference of a flow solution, provided the wave number vector of the solution is the same as the wave number vector of one of the mode generating the shape of the corrugated boundary. Application of Riahi's theory (2001) to wind flow was given in Riahi (2007).

In the present study, we consider a different type of resonance condition where the wavelength of a mode, which is generated either by a particular discrete structure in the form of a hump or entirely due to another discrete structure in the form of a segment of a discrete wave, is equal to half of the wavelength of the critical mode for the channel flow. We carry out both qualitative and quantitative studies for the resulting flow systems and find some interesting results. In particular, we find that such resonance condition leads to the existence of a steady flow in same subcritical domain. This steady flow has the same horizontal scale as either of the wave structure or as one of the Fourier mode of the hump structure.

2. Governing System

We consider the governing partial differential equation for momentum and mass conservation (Batchelor, 1970) for a horizontal channel flow of depth d between two flat boundaries. We

assume that over the lower boundary of the channel, there is a small stationary discrete structure. We regard the layer of fluid as incompressible with constant density ρ.

We consider a Cartesian system of coordinate x^*, y^*, z^*, with z^*=0 being the location of the bottom boundary of the channel. We non-dimensionalize the governing partial differential equations by using d, U, d/U and ρU^2 as scales for length, velocity, time and modified pressure, respectively. Here, U is the appropriate velocity scale which is chosen here to be the maximum mean values of flow speed across the fluid layer. The non-dimensional form of the governing equations [Batchelor (1970)] can then be written in the form

$$(\frac{\partial}{\partial t} + \mathbf{u}.\nabla)\,\mathbf{u} = -\nabla P + (\frac{1}{R})\nabla^2\mathbf{u}, \tag{1a}$$

and

$$\nabla.\mathbf{u}=0. \tag{1b}$$

Here, $\mathbf{u}$= (u, v, w) is the velocity vector, P is the modified pressure, t is the non-dimensional time variable and $R=Ud/\nu$ is the Reynolds number, where ν is the kinematic viscosity. In general the non-dimensional dependent variables $\mathbf{u}$ and P are functions of the non-dimensional independent variables x, y, z and t.

We shall measure the strength of the flow in terms of its maximum speed U only, so that the layer thickness d is assumed to be fixed. We designate the original basic state velocity vector and the modified pressure gradient for the channel flow, which exist initially in the absence of any perturbation, by $\mathbf{u}_b$ and P_b, respectively. The basic state velocity vector is that due to the unidirectional channel flow driven by a constant pressure gradient in the horizontal direction (Batchelor, 1970). Hence, both the basic state velocity vector and the basic state pressure gradient are in the horizontal direction. The basic state solutions are derived from (1a-b) by assuming that the basic state velocity vector and pressure are, respectively, only functions of z and x. Their expressions are known to be [Drazin and Reid (1981)]

$$\mathbf{u}_b = 4(z - z^2)\,\mathbf{x}, P_b = (\frac{8}{R})x + P_o, \tag{2a-b}$$

where $\mathbf{x}$ is a unit vector in the direction of horizontal x-axis, x is the horizontal variable and P_o is a constant. Figure 1 presents the horizontal basic state velocity profile.

We assume that the height δ in the z-direction of the surface structure is small (δ<<1). We now write $\mathbf{u}=\mathbf{u}_b+\mathbf{u}'$ and $P=P_b+P'$, where $\mathbf{u}'$ and P′ are, respectively, the velocity vector and the modified pressure for the perturbations superimposed on the basic flow. The governing partial differential equations for the perturbation variables can then be obtained by using the above expressions for $\mathbf{u}$ and P in the equations (1a-b) and subtracting from the resulting equations the corresponding equations for the basic flow. The resulting equations for the perturbation variables are

$$(\frac{\partial}{\partial t}+\mathbf{u}_b.\nabla)\,\mathbf{u}'+\mathbf{u}'.\nabla\mathbf{u}_b+\nabla P'-(\frac{1}{R})\nabla^2\mathbf{u}'=-\mathbf{u}'.\nabla\mathbf{u}', \tag{3a}$$

and

$$\nabla.\mathbf{u}'=0. \tag{3b}$$

The boundary conditions for (3a-b) are

$$\mathbf{u}'=-\sum_{m=1}\,[\frac{(\delta h)^m}{m!}](\frac{\partial^m}{\partial z^m})\,(\mathbf{u}_b+\mathbf{u}')\text{ at } z=0, \tag{3c}$$

$$\mathbf{u}'=0\text{ at } z=1, \tag{3d}$$

where $h(\boldsymbol{r})$ is the shape function for the discrete structure, which is, in general, a function of the horizontal variable vector $\boldsymbol{r}=(x, y)$, and δh is the structure height. Here δ represents the order of magnitude of the height of the structure, which is assumed to be small ($\delta<<1$). We have assumed that the boundary conditions for the total velocity vector **u** are prescribed constants equal to the corresponding basic state values. Conditions (3c-d) are obtained by the consideration that the imposed structure on the lower boundary introduce simply surface perturbations which contribute to the disturbance system only [Riahi (2001)], and such contribution is of main interest in the present study. The terms in the right-hand side of (3c) arise simply by the contributions of the higher-order terms in a Taylor-series expansion about $z = 0$ of the total velocity vector, which are due to the surface structure.

3. Analysis and Results

3.1. Analysis and General Results

We assume that the shape function for the surface structure can be represented by

$$h(\boldsymbol{r})=\sum_{n=-M}^{M} A_nE_n \equiv\sum_{n=-M}^{M} A_n\exp(i\boldsymbol{j}_n.\boldsymbol{r}), \tag{4}$$

where $i=\sqrt{-1}$, M is a positive integer, which may be sufficiently large for particular structures, and the horizontal wave number vectors $\boldsymbol{j}_n=(\tilde{\alpha}_n\,,\,\tilde{\beta}_n)$ of the structure satisfy the properties

$$\boldsymbol{j}_{-n}=-\boldsymbol{j}_n. \tag{5}$$

The amplitude coefficients A_n satisfy the condition

$$A_n^{*}=A_{-n}, \tag{6}$$

where "asterisk" indicates complex conjugate. Conditions (5)-(6) ensure that expression (4) for h is real. The expression (4) for h, which is referred to here as the modal representation for the shape function of the discrete structure, is assumed in this paper.

We consider the so-called critical regime where the domain of the flow corresponds to the values of the Reynolds number (sufficiently close to its critical value) below which no disturbances are linearly unstable ($R \approx R_c$). We also take note of the qualitative cases of modulated boundary temperature in thermal convection [Riahi (1995)] and surface corrugation in shear flows [Riahi (2001)], where certain domain in the order of magnitude of the disturbances relative to the size of the magnitude of the modulated boundary temperature or corrugated surface was detected under which new type of flow resonance can be explored. We then find that the corresponding regime for the present qualitative and quantitative study is

$$O(\delta) < \varepsilon < O(\delta^{1/2}), \tag{7}$$

where ε is the magnitude of the amplitude of the perturbation motion. As will be seen later, under (7) we detected, in particular, a resonance condition where a wave number vector of the perturbation can balance superposition of two wave number vectors of the discrete boundary structure.

Applying the weakly nonlinear theory [Drazin and Reid (1981)], we define a slowly varying time τ

$$\tau = \delta t, \tag{8}$$

and pose double expansions in powers of ε and δ for $\mathbf{u}'$, P' and R

$$(\mathbf{u}', P', R) = \sum_{m,n} \varepsilon^m \delta^n (\mathbf{u}_{mn}, P_{mn}, R_{mn}), \quad \mathbf{u}_{00} = P_{00} = 0. \tag{9a-b}$$

We use (2) and (8)-(9) in (3). In the order $\varepsilon^1 \delta^0$, we find the linear system for $\mathbf{u}_{10}$ and P_{10}. This system admits solution of the form

$$(\mathbf{u}_{10}, P_{10}) = \sum_{n=-N}^{N} [\mathbf{u}_{10n}(z), P_{10n}(z)] B_n F_n, \; F_n \equiv \exp[i(\boldsymbol{k}_n . \boldsymbol{r} - \omega_n t)], \tag{10a-b}$$

where N is a positive integer, and the amplitude function $B_n(\tau)$ satisfies condition of the form (6) that was satisfied by A_n. The real frequency ω_n and the horizontal wave number vectors $\boldsymbol{k}_n = (\alpha_n, \beta_n)$ of the perturbation satisfy the condition of the form (5) that was satisfied by $\boldsymbol{j}_n$. The coefficient functions $\mathbf{u}_{10n}$ and P_{10n} satisfy the condition of the form (6) and are obeyed by a system with zero boundary conditions, which can be derived by using (10) in the linear system in the order ε. This system of ordinary differential equations and similar types of systems, which are involved in the present study, will not be given here but will be reported elsewhere.

The weakly nonlinear method requires us to consider the adjoint linear system whose solution can be written in the form

$$(\mathbf{u}_{10}^{\wedge}, P_{10}^{\wedge}) = \sum_{n=-N}^{N} [\mathbf{u}_{10n}^{\wedge}(z), P_{10n}^{\wedge}(z)] B_n F_n^{\wedge}, \; F_n^{\wedge} \equiv \exp[i(\boldsymbol{k}_n . \boldsymbol{r} + \omega_n t)], \tag{11a-b}$$

where the above z-dependent coefficients satisfy the condition of the form (6) and are obeyed by a linear system with zero boundary conditions, which will not be given here but will be reported elsewhere. In the order $\varepsilon^0\delta^1$, the governing equations and the upper boundary conditions are of the same form as the corresponding ones in the order ε, provided ($\mathbf{u}_{10}$, P_{10}) is replaced by ($\mathbf{u}_{01}$, P_{01}). The lower boundary conditions are, however, of the order δ version of (3c), provided $\mathbf{u}'$ is replaced by $\mathbf{u}_{01}$. This system admits solution of the form

$$(\mathbf{u}_{01}, P_{01})=\sum_{n=}^{M}{}_{-M} [\mathbf{u}_{01n}(z), P_{01n}(z)]A_nE_n, \tag{12a}$$

where the equations and the upper boundary conditions for the coefficient functions ($\mathbf{u}_{01n}$, P_{01n}) are of the same form as the corresponding ones for ($\mathbf{u}_{10n}$, P_{10n}) described before, provided $\boldsymbol{k}_n$ is replaced by $\boldsymbol{j}_n$ and ω_n by 0. However, the lower boundary condition is now

$$\mathbf{u}_{01n}=-d\mathbf{u}_b/dz \quad \text{at } z=0. \tag{12b}$$

Forming the solvability condition, which states that non-homogeneities must be orthogonal to the solution of the adjoint linear system [Drazin and Reid (1981)] for the order ε^2 system, we find $R_{10}=0$. Using (7), we find that R_{01} is the leading coefficient beyond R_{00} in the expansion (9a) for R, and it is found that it can be non-zero and appears in the solvability condition for the εδ-system. This condition can then be reduced to the following system of ordinary differential equations for B_n

$$(\frac{\partial}{\partial\tau}-R_{01}\,a_n)B_n=\sum_{m,\,p} b_{nmp}\,B_pA_m\langle F_n^{\wedge *}F_pE_m\rangle,\ (n=-N, \ldots, -1, 1, \ldots, N), \tag{13a}$$

where the angular bracket $\langle\ \rangle$ denotes an average over the fluid layer defined by

$$\langle f\rangle\equiv\lim_{L\to\infty}[1/(2L)]\int_{-L}^{L} dx\int_0^1 f\,dz. \tag{13b}$$

The expressions for the constant coefficients a_n and b_{nmp} in (13a), which are in terms of integrals involving solutions of the perturbation systems at the orders $\varepsilon^1\delta^0$ and $\varepsilon^0\,\delta^1$ and solution of the adjoint system, are generally lengthy and will not be given here, but they will be reported elsewhere.

To distinguish the physically realizable solutions(s) among all the solutions of (13a), the stability of B_n (n=-N, …, -1, 1, …, N) with respect to the amplitude functions $C_n(\tau)$ for new disturbances superimposed on B_n and subjected to (13a) are investigated. To find the equations for the amplitude functions $C_n(\tau)$, we assume that the functions (B_n+C_n) satisfy (13a). Subtracting the equations (13a) from the corresponding equations for these functions, we find the system of the ordinary differential equations for the time-dependent disturbances in the form

$$(\frac{\partial}{\partial\tau}-R_{01}\,a_n)C_n=\sum_{m,\,p} b_{nmp}A_mC_p\langle F_n^{\wedge *}E_m\,F_p\rangle,\quad (n=-N, \ldots, -1, 1, \ldots, N), \tag{14}$$

where C_n also satisfies the condition of the form (6).

It can be seen from (13a) and (14) that the height of the surface structure affects the channel flow solution and the disturbances through the terms containing R_{01}, while the shape of the surface structure affects the channel flow solution and the disturbances through Fourier coefficients A_mE_m (m=-N, …, -1, 1, …, N), which enter as the source term in the right-hand-side in (13a) and (14), respectively. It is seen from (13a) that the height of the structure is effective only if $R_{01}\neq 0$, while the shape of the structure can be effective only if the source term in the right-hand-side in (13a) is non-zero. The integral expression $<F_n^{\wedge *}E_mF_p>$ in (13a) or in <14> is non-zero only if

$$\boldsymbol{k}_n=\boldsymbol{j}_m+\boldsymbol{k}_p \quad \text{and} \quad \omega_n=\omega_{-p}, \tag{15a}$$

or, in particular, if

$$\boldsymbol{j}_{-m}=2\,\boldsymbol{k}_p \text{ and } n=-p, \tag{15b}$$

for at least some m and p. For a significant surface structure, it is possible to choose A_m appropriately to achieve either oscillatory (in time) solutions B_n for (13a) where a time dependence of the form $\exp(\sigma\tau)$ is assumed for B_n or steady solutions B_n for (13a). For such types of solutions for (13a), the $N\times N$ determinant of the coefficients for B_n (n=1, …, N) in (13a) must vanish. It is also found from (13a) and (14) that if B_n decreases indefinitely with increasingτ, then the order-ε solution decays to zero and the stable solution is that due to the induced flow system at order δ, while the induced flow is unstable if B_n increases indefinitely with τ.

3.2. Specific Results

In the present paper, we studied two types of two-dimensional surface structures and two-dimensional flow solution in (x, z)-plane for (13a) for the simplest case where N = 1. Thus, $\mathbf{J}_1=2\mathbf{k}_1$, $\tilde{\alpha}_1=2\alpha_1$, $\tilde{\beta}_1=\beta_1=0$, and (15a) reduces to (15b). It should also be noted that the two-dimensional flows and structures that are studied in this paper can be considered as the corresponding ones in the realistic three-dimensional domain, provided no variation for such flows and structure can exist in the third dimension. We consider a particular hump type structure (Figure 2) whose shape function can be in the following form:

$$h(x)=\frac{1}{\cosh(5x)},\ -2L\le x\le 2L,\ L=\frac{\pi}{4\alpha_1}. \tag{16a-c}$$

The Fourier coefficient A_{12} given in (4) for h(x) is then obtained from [Greenberg (1998)]

$$A_{12}=[1/(4L)]\int_{-2L}^{2L} h(x)\cos[2x/(2L)]\mathrm{d}x \tag{17a}$$

giving the value of

$$A_{12}=0.014. \tag{17b}$$

This particular coefficient for $n = 12$ was needed since it enters in the right-hand-side of (14) and only in the term that is non-zero because of our specific case here and the results given in (15). Thus, in the modal representation (4) for the shape function of such hump type structure, only one Fourier mode corresponding to $n = 12$ in (4) can have non-zero contribution in the present study. We also consider another type of surface structure in the form of a wave segment (Figure 3) whose horizontal wavelength is the same as the one due to this particular Fourier mode of the hump structure with coefficient A_{12} given by (17b). We have chosen this second surface structure because of particular resonance condition (15b) and the domain (16b-c) which will be seen in this section to lead to preference of a steady flow due to such structure.

From the careful and notable work by Hocking and Stewartson (1972), we have

$$R_c=11548,\ \alpha_1=1.0202,\ \beta_1=0,\ \omega_1=0.264\alpha_1. \tag{18a-d}$$

We carried out numerical computation using an efficient fourth order Runge-Kutta algorithm [Ascher et al. (1995); Cheney and Kincaid (2008)] to generate data for the eigenfunctions $\mathbf{u}_{101}(z)$ and $P_{101}(z)$ with the given values in (18) for the corresponding eigenvalue problem, which were already obtained by Hocking and Stewartson (1972). Because of known eigenvalue and the corresponding data given in (18) that we used, our numerical problem was relatively simpler than the full eigenvalue problem with unknown eigenvalues computed by Davey (1973) who used orthonormalization to solve Orr-Sommerfeld problems [Drazin and Reid (1981)] even though the method of approach was turned out to be a simple parallel shooting type procedure [Ascher et al. (1995)]. We implemented the Runge-Kutta algorithm by first converting the equations for $\mathbf{u}_{101}$ and P_{101} into a system of four ordinary order differential equations and then following a numerical shooting approach [Ascher et al. (1995)] and using the eigenvalue data (18), we carried out computation and generated data for the corresponding eigenfunctions. Similarly, we generated numerical data for the solutions $\mathbf{u}_{101}\hat{}(z)$, $P_{101}\hat{}(z)$, $\mathbf{u}_{011}(z)$ and $P_{011}(z)$ as the z-dependent coefficients in (11)-(12) for $n = 1$. We used these data and Simpson's rule [Atkinson (1989)] to compute the values of the coefficients a_1 and $b_{1m,-1}$ in (14) for $n = 1$ and $p = -1$ since the expressions for these coefficients were given in terms of integrals involving the eigenfunctions and the solutions referred to above. We found the following values for these coefficients:

$$a_1=0.0313-0.1786i,\ b_{1m,-1}=-0.0019-0.0122i. \tag{19a-b}$$

Using (17) and (19) in (13) for $n = 1$ and $p = -1$, we find the equation for B_1 in the form

$$\left(\frac{\partial}{\partial\tau}-a_1R_{01}\right)B_1=b_{1m,-1}A_{12}\,B_1^*, \tag{20}$$

and together with a corresponding equation for B_1^* lead to a solution for B_1 in the form

$$B_1=B_{10}\exp(s\tau), \tag{21a}$$

where B_{10} is a constant and the growth rate s is given by

$$s^2 - 2 R_{01} a_{1r} s + (|a_1|^2 R_{01}^2 - A_{12}^2 |b_{1m,-1}|^2) = 0, \quad (21b)$$

where a_{1r} is the real part of a_1. Using (17b) and (19) in (21b), we find that

$$s_r < 0 \text{ if } R < R_c - 0.001\delta, \quad (22a)$$

$$s_r = 0 \text{ if } R = R_c - 0.001\delta, \quad (22b)$$

and

$$s_r > 0 \text{ if } R > R_c - 0.001\delta, \quad (22c)$$

where s_r is the real part of s.

Following the results presented in the sub-section 3.1 and (22a-b) it follows that the perturbation grows in time and unstable if (22c) holds, the total induced oscillatory flow, as the sum of the solutions at the orders ε and δ, is marginally stable if (22b) holds, while the induced steady flow at order δ is stable in the subcritical domain given in (22a). The subcritical domain (22a) and its upper boundary (22b) are predicted based on the particular Fourier mode of the solution at order δ whose wave number vector satisfies the resonance condition (15b). As we have shown, this Fourier mode, which is referred to here as an effective mode, is due to either only one of the mode of the hump structure or entirely due to the wave-segment structure. Figures 4a and 4b present, respectively, the horizontal component u_{01} of the velocity vector for the induced steady flow due to the wave-segment structure, but they also due to this effective Fourier mode versus the horizontal variable and for several values of the vertical level z.

We have rescaled x with respect to the wavelength, so that the rescaled X is given by $x/(\alpha_1/\pi)$. Thus, as can be seen from the Figure 4a, the horizontal length scale exhibited by such flow is the same as that due to the wave-segment structure and is half of $(2\pi/\alpha_1)$, which was due to the critical flow at $R = R_c$ and in the absence of the structure. The result shown from the figure 4b indicates that variation of u_{01} is essentially linear with respect to z with rate of variation depending on the value of X. Figures 5a and 5b are the same as the Figures 4a-b, respectively, but for the vertical component w_{01} of the velocity vector for the same flow and with results analog to those shown in the Figure 5a. Since the actual values of w_{01} were quite small, the associated figures are shown for rescaled values of w_{01} equal 10^4 of those actual values.

It can be seen from these figures that the X-dependence results for w_{01} are analog those for u_{01} which were provided for the figure 4a, but the z-variation results are not linear in general. Figures 6a and 6b present, respectively, three-dimensional surfaces for u_{01} and w_0 as functions of X and z. Both X and z dependence of these quantities that appear clearly in single figures, are the accumulated results we explained before from Figures 4-5.

In regard to roles played by the hump type structure in the flow solution, it should be noted that the present study is restricted to the case $N = 1$, where in the right-hand-side of equation (10a) only one term plus its complex conjugate term are retained. Under such case, we found that the

flow solution subjected the whole shape function of the wave-segment structure is the same as the one due to only one mode, which we referred to earlier as the effective mode, of the hump structure.

Other modes in the expression (4) for the hump structure have no contribution to the flow solution. This is due to the method of solution for the present study where the modal representation for both structure and flow solution are considered. Thus, a flow solution due to the entire form of the shape function for the hump structure given by (16a), which in the modal representation can involve infinite number of modes [$M = \infty$ in (4)] is not possible based on the present approach and is beyond the scope of the present study.

4. Concluding Remarks

The results of the present qualitative and quantitative investigation of the effect of discrete surface structures on the channel flow, which was based on particular mathematical model, indicate that the surface structure can have significant influence on the amplitude, scales, pattern and secondary mode excitation of the channel flow. Under certain resonance condition, where the wavelength of either an entire wave-segment structure or a particular Fourier mode of a hump type structure equal to half that of the critical mode of the channel flow in the absence of the structure, we found that an induced steady flow can be developed for R slightly less than its critical value.

The main results of the present study are that the channel flow can be manipulated by a structured surface, shear flow modes can be enhanced by a structure surface, larger height of the structure can affect the flow more significantly, the generated flow takes on the scale of the structured surface mode and length scale is reduced due to the structured surface. These results are all in good agreement with the available experimental results [Muller and Bippes (1988); Rodeztsky (1994); Tomkin (2000)].

The results presented in this paper indicate significance of the presence of the surface structure on the development of stable flow and the roles played by a given discrete structure in developing a stable flow regime. It is hoped that such results can be stimulated for future research studies for constructing structures that can predict outcome of certain induced shear flows over such structures.

Stationary surface structures, such as those considered here, can likely to affect the spatial features of the channel flow. It should be noted that even though the induced flow solutions, can, in general, be due to both steady and time-dependent modes, the stationary surface structures can be effective only on the steady modes of the channel flow.

The present study was restricted to stationary surface structures, discrete stationary modes and certain resonant mode excitation. Further extensions of the present study, might in the future studies, include both qualitative and quantitative studies for cases of specific moving discrete or non-discrete surface structures and non-discrete [Riahi (1996)] stationary or non-stationary modal cases.

Acknowledgement

This research was supported by a grant from UTPA-FRC.

REFERENCES

Angelis, V. D., Lombardi, P. and Banerjee, S. (1997). Direct Numerical Simulation of Turbulent Flow Over a Wavy Wall, Physics of Fluids, **9**, pp. 2429-2442.

Ascher, U. M., Mattheij, R. M. M. and Russell, R. D. (1995). Numerical Solution of Boundary Value Problems for Ordinary Differential Equations, SIAM, Philadelphia.

Atkinson, K. A. (1989). An Introduction to Numerical Analysis, Second Edition, John Wiley & Sons, Inc., New York.

Batchelor, G. K. (1970). An Introduction to Fluid Dynamics, Cambridge Univ. Press, UK

Cheney, W. and Kincaid, D. (2008). Numerical Mathematics and Computing, Sixth Edition, Thomson Brooks Co., Stamford, CT.

Davey, A. (1973). A simple numerical method for solving Orr-Sommerfeld problems, Quarterly J. Mech. Appl. Math, **26**, pp. 401-411.

Drazin, P. G. and Reid, W. H. (1981). Hydrodynamic Stability, Cambridge Univ. Press, UK.

Greenberg, M. D. (1998). Advanced Engineering Mathematics, Second Edition, Prentice Hall, U.S.A.

Hocking, L. M. and Stewartson, K. (1972). On the nonlinear response of a marginally unstable plane parallel flow to a two-dimensional disturbance, Proc. R. Soc. Lond. A **326**, pp. 289-313.

Hudson, J. D., Dykhvo, L. and Hanratty, T. J. (1996). Turbulence Production in Flow Over a Wavy Wall, Experiments in Fluids, **20**, pp. 257-265.

Krettenauer, K. and Schumann, U. (1992). Numerical Simulation of Turbulent Convection Over Wavy Terrain, J. Fluid Mechanics, **237**, pp. 261-299.

Morkovin, M. V. (1983). Understanding Transition to Turbulence in Shear Layers, Defence Technical Information Center, and U.S. A.

Muller, B. and Bippes, H. (1988). Experimental Study of Instability Modes in a Three-dimensional Boundary Layer, In Fluid Dynamics of Three-Dimensional Turbulent Shear Flows, AGARD CP438.

Riahi, D. N. (1995). Finite Amplitude Thermal Convection with Spatially Modulated Boundary Temperatures, Proc. of the Royal Society of London, Series A, **449**, pp. 459-478.

Riahi, D. N. (1996). Modal Package Convection in a Horizontal Porous Layer with Boundary Imperfections, J. Fluid Mechanics, **318**, pp. 107-128.

Riahi, D. N. (1997). Effects of Roughness on Nonlinear Stationary Vortices in Rotating Disk Flows, Mathematical and Computer Modeling, **25**, pp. 71-82.

Riahi, D. N. (2001). Effects of Surface Corrugations on Primary Instability Modes in Wall Bounded Shear Flows, Nonlinear Analysis: Real-World Applications, **2**, pp. 105-133.

Riahi, D. N. (2007). Mathematical modeling of wind forces, Int. J. Applied Math. & Statistics, **10(S07)**, pp. 70-80.

Rodeztsky, R. H., Reibert, M. S. and Saric, W. S. (1994). Development of Stationary Crossflow Vortices on a Swept Wing, AIAA paper 94-2373.
Schlichting, H. (1979). Boundary Layer Theory, 7th Edition, McGraw-Hill Co., U. S. A.
Tomkin, C. D. (2000). The Structure of Turbulence Over Smooth and Rough Walls, PhD Thesis, University of Illinois at Urbana-Champaign, U. S. A.

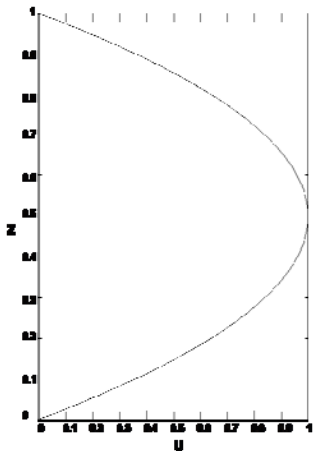

Figure 1. Base flow velocity component in the horizontal direction versus *z*

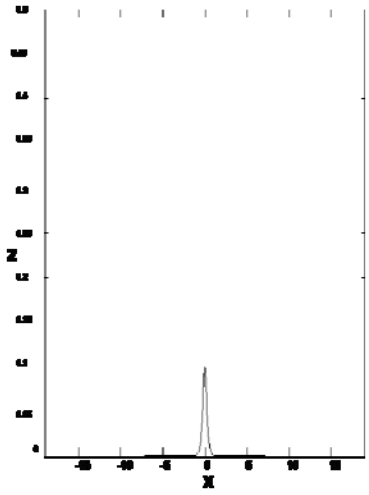

Figure 2. The shape of a hump type surface structure in the (*x*, *z*)-plane

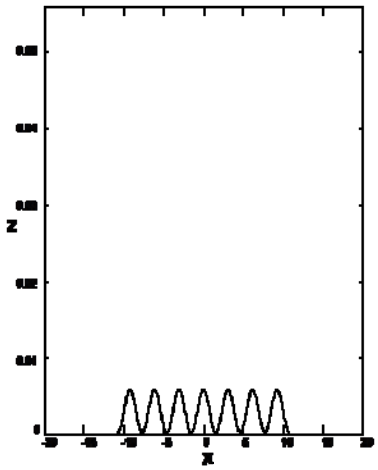

Figure 3. The shape of a wave-segment type surface structure in the (*x*, *z*)-plane

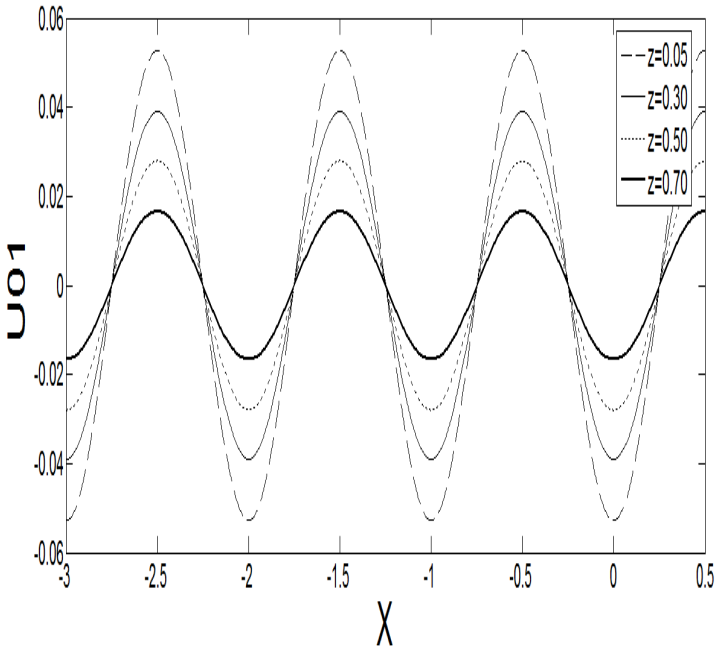

Figure 4a. Horizontal component of the induced steady flow versus scaled horizontal variable *X* for several values of *z*.

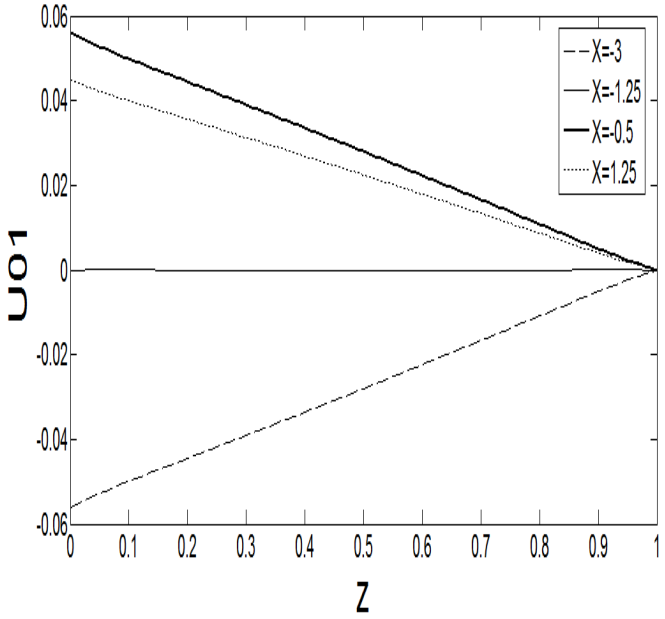

Figure 4b. The same as in the figure 4a but versus z for several values of *X*

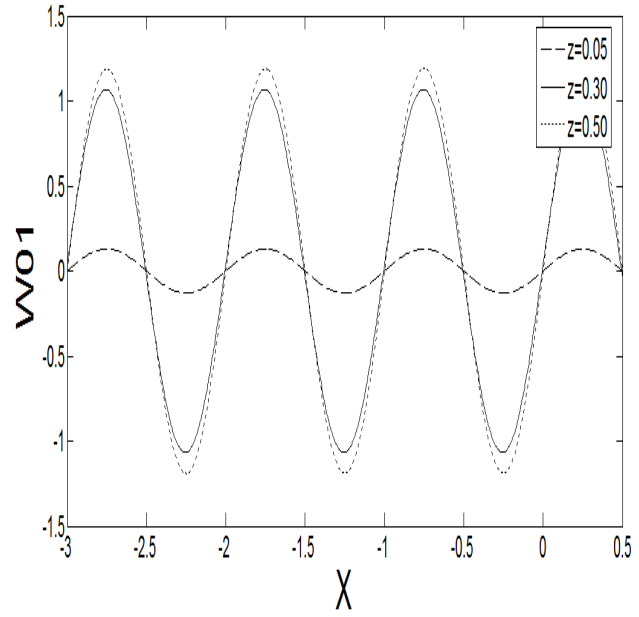

Figure 5a. Vertical component of the induced steady flow versus *X* for several values of z

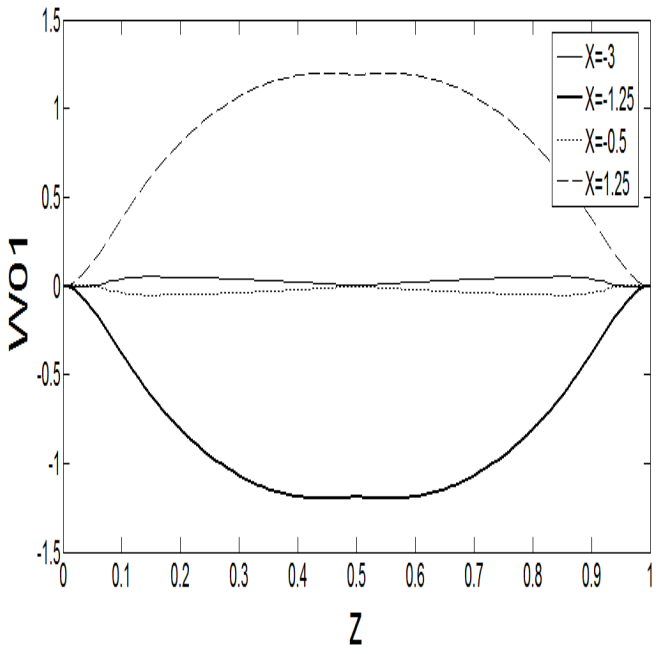

Figure 5b. The same as in the figure 5a but versus *z* for several values of *X*

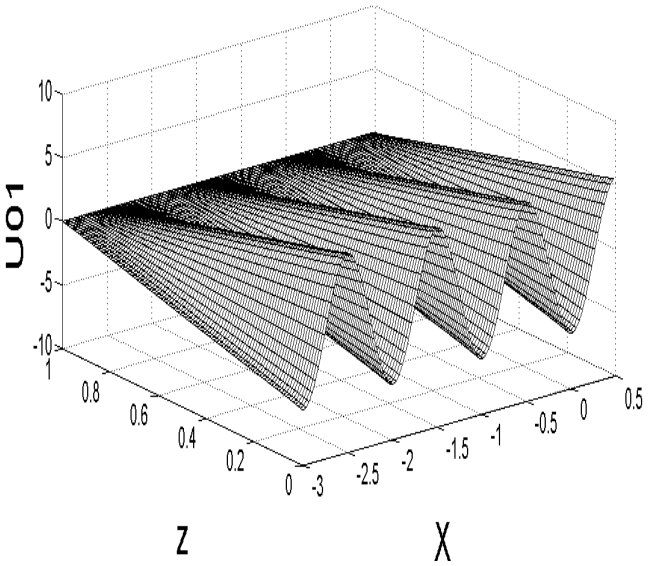

Figure 6a. Three-dimensional view of the horizontal component of the induced steady flow versus *X* and *z*

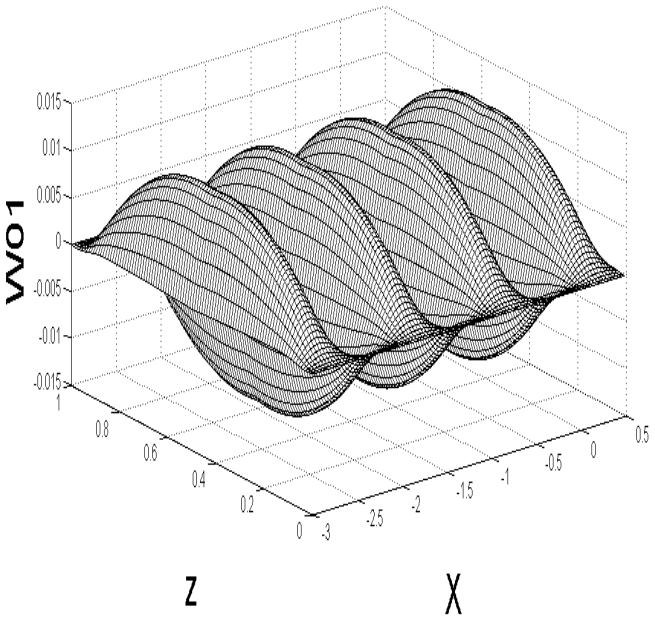

Figure 6b. The same as in the figure 6a but for the vertical component of the induced steady flow